Interference of citrate-stabilized gold nanoparticles on β2-microglobulin oligomeric association

Cristina Cantarutti,[a] Gijo Raj,[b] Federico Fogolari,[c,d] Sofia Giorgetti,[e] Alessandra Corazza,[a,c] Vittorio Bellotti,[e,f] Panče Naumov[b] and Gennaro Esposito*[b,c,d]

Protein fibrillation is involved in many seriuos diseases and protein oligomers proved to be precursors of amyloid fibrils. NMR and QCMD experiments allowed us to establish that the interaction between citrate-stabilized gold nanoparticles and a paradigmatic amyloidogenic protein, β2-microglobulin, is able to interfere with protein association into oligomers.

The involvement of protein fibrillation has been established in several pathologies, e.g. Alzheimer's and Parkinson's diseases, type II diabetes and dialysis-related amylodosis.[1–3] Although the exact pathway leading from monomeric polypeptides to fibrillar assemblies is not yet fully understood, there is general agreement on the occurrence of intermediate misfolded states that are capable to nucleate into oligomers of various molecular weights.[4–7] Furthermore, for some proteins, the protofibrillar aggregates show an enhanced toxicity compared to the mature fibrils.[7,8] Therefore, targeting early oligomeric species is of relevance to the design of strategies for amyloidosis treatment. Among the well identified amyloidogenic proteins, β2-microglobulin (β2m) has been extensively studied not only because it is responsible for dialysis-related amyloidosis (DRA), but also because it recapitulates the characteristic features of the amyloidogenic proteins.[9,10] β2m is the non-polymorphic light chain of class I major histocompatibility complex that accumulates in the blood and eventually converts into fibrils in patients with chronic renal failure,.[9,10] A hereditary systemic amyloidosis has also been reported[11] which is due to a naturally occurring β2m variant, namely D76N where the Asp in position 76 is mutated into Asn. D76N β2m is much more amyloidogenic and exhibits substantially lower thermodynamic stability compared to the wild-type (WT) protein, even though both species have identical three dimensional structure.[12] We have recently demonstrated that citrate-stabilized gold nanoparticles (Cit-AuNP) are able to hinder D76N β2m fibrillogenesis *in vitro* through a mechanism that likely entails a competitive interference at the level of the early aggregation events.[13] The ability of nanoparticles (NP) to affect protein fibrillation process, either by inhibiting or by promoting it, has been repeatedly reported, however detailed explanation of the mechanisms is still lacking.[14]

Here, we present the investigation of the effect of Cit-AuNP on the association equilibria of β2m variants. Measurements were carried out by NMR spectroscopy and Quartz Crystal Microbalance with Dissipation monitoring (QCMD) experiments.§ To the aim, Cit-AuNP with average diameter of 7.5 nm were synthesized (Fig. S1, ESI†) and their interaction with WT and D76N β2m was preliminarily tested through two-dimensional NMR. We recorded ^{1}H-^{15}N HSQC[15] spectra of β2m variants in absence and in presence of Cit-AuNP, at two different protein/NP ratios, i.e. 680 and 160 (Fig. 1, for the full spectra see Figs. S2-S5, ESI†). The analysis of the spectra showed, for all the tested samples, only small meaningful deviations ($\Delta\delta$) of the cumulated chemical shift values,[16] (Fig. S6-S9, ESI†). For both WT and D76N, an unevenly distributed intensity attenuation was observed with Cit-AuNP. The average relative intensities in presence of Cit-AuNP were for WT 0.76±0.075 and 0.71±0.13 at 680 and 160 protein/NP ratios, respectively. With D76N, the average relative intensities were 0.79±0.064, and 0.50±0.070 at the higher and lower protein/NP ratio, respectively. In general, the intensity attenuation is quite constant even when the protein/NP ratio is decreased. This behaviour was observed previously for both D76N and WT β2m.[13,17] The intensity attenuation measured here for D76N at the lower protein/NP ratio depends on the specific protein batch used for NMR samples that showed some peak splittings and the onset of non-native peaks (Fig. S5, ESI†). The repeated observations of a single resonance without significant $\Delta\delta$ for the backbone amide signals[13,17]

[a] *DAME, Università di Udine, P.le Kolbe 4, 33100 Udine, Italy.*
[b] *New York University Abu Dhabi, PO Box 129188, Abu Dhabi, UAE.*
[c] *INBB, Viale Medaglie d'Oro 305, 00136 Roma, Italy.*
[d] *DMIF, Università di Udine, Viale delle Scienze, 33100 Udine, Italy.*
[e] *Dipartimento di Medicina Molecolare, Università di Pavia, Via Taramelli 3, 27100 Pavia, Italy*
[f] *Division of Medicine, University College of London, London NW3 2PF, UK.*

† Electronic Supplementary Information (ESI) available: Cit-AuNPs synthesis and characterization, NMR and QCMD experimental details, full ^{1}H-^{15}N HSQC NMR spectra, NH cross-peak relative intensity and chemical shift perturbation bar plots, QCMD graphs for Cit-AuNP and β2m structure. See DOI: 10.1039/x0xx00000x

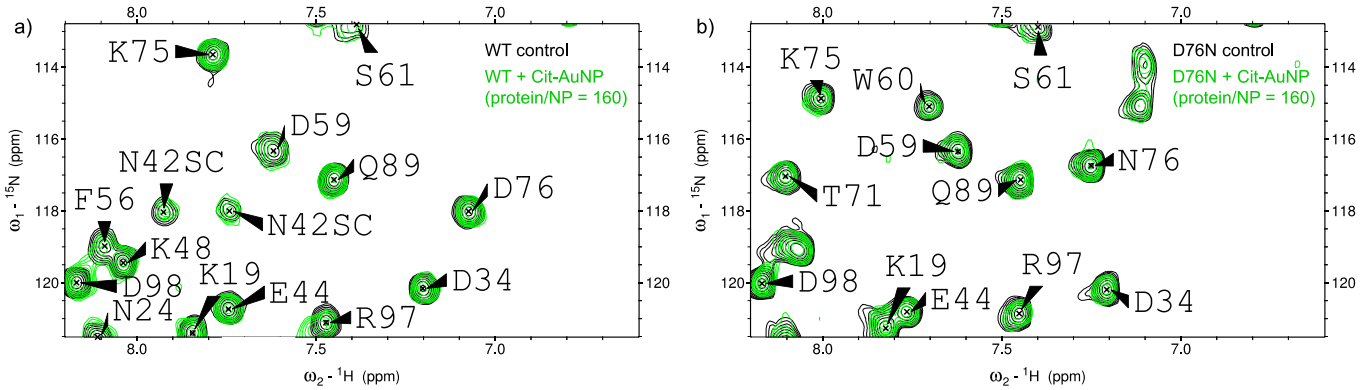

Fig. 1 Region from the overlay of ^{15}N-^{1}H HSQC spectra of 4 µM β2m without (black contours) and with (green contours) 25 nM Cit-AuNP for a) WT and b) D76N. SC indicates side-chain NH connectivities. The whole maps are reported in Figs. S3 and S5 (ESI†).

suggest that the interaction between the two β2m variants and Cit-AuNP is transient (fast exchange) and does not affect the overall protein structure.

To assess the effect of Cit-AuNP on β2m association equilibria, the translational diffusion coefficients of WT and D76N β2m variants with and without Cit-AuNP (protein/NP = 160) were estimated by means of DOSY experiments.[18] It has been already reported that, in β2m solutions, monomers are in equilibrium with oligomers of variable stoichiometry leading to a weighted-average single diffusion coefficient.[19,20] We found that Cit-AuNP increase the diffusion coefficients of the two considered β2m variants (Fig. 2). The effect was more pronounced with the more amyloidogenic variant, but definitely appreciable also for WT β2m. However the large signals from buffer and citrate (mM) hinder quantitative analysis of the protein signals (µM). The increase of the diffusion coefficient suggests a shift of β2m association equilibria towards lower oligomers and is consistent with previous molecular dynamics results in which D76N β2m dimers appeared to split in presence of Cit-AuNP.[13]

Subsequently, we performed QCMD experiments to measure the changes in the resonance frequency (Δ*f*) of an oscillating quartz crystal positioned between two electrodes when 1 µM D76N β2m, in absence and in presence of 25 nM Cit-AuNP, was flowed onto an Au-coated QCMD sensor. The NP concentration was the same as used in any NMR sample, whereas the protein solution was freshly prepared from a

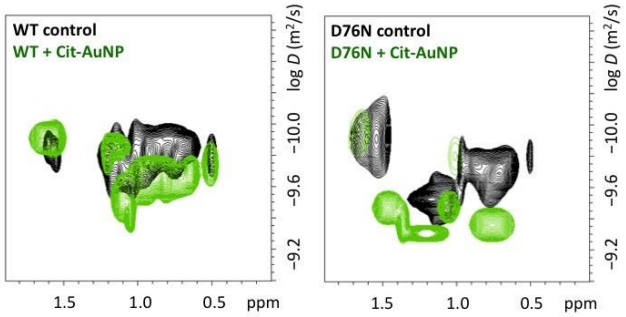

Fig. 2 Overlay of DOSY spectra of the aliphatic region of WT (left panel) and D76N (right panel) β2m recorded without (black) and with (green) Cit-AuNP.

controlled batch and at a fourfold dilution with respect to the lowest concentration that was examined by NMR.

The quartz microbalance frequency variation is proportional to the mass density (*Δm*) in ng·cm^{-2} of the adsorbed material through the Sauerbrey equation:[21]

$$\Delta f = -nC\Delta m \qquad (1)$$

where n is the vibrational overtone considered (the fifth, in our setting) and C is a constant that depends on instrument characteristics (17.8 ng cm^{-2} Hz^{-1}). In addition to Δ*f*, also the changes in dissipation, Δ*D*, due to adsorption of the two samples were recorded. The energy dissipation recorded during the adsorption reflects the stiffness of the material that contacts the sensor surface. The plots of Δ*f* and Δ*D* as a function of time are shown in Fig. 3. The saturation Δ*f* (Δf_{sat}) and Δ*D* (ΔD_{sat}) values are reported in Table 1. The differences in Δf_{sat} and ΔD_{sat} observed for D76N β2m in presence and in absence of Cit-AuNP are significant, since the noise level associated with frequency and dissipation measurements are very low, i.e. ±0.1 Hz and ±1×10^{-7} dissipation units, respectively.[22] The frequency shift was fitted with the Sauerbrey equation[21] to calculate the areal mass density (Fig. 4a). From the areal mass density and the protein molecular mass, it was possible to calculate the surface coverage density in terms of protein monomers/cm^2 (Table 1). For the protein alone, a higher surface coverage was obtained (14.5×10^{12}) with

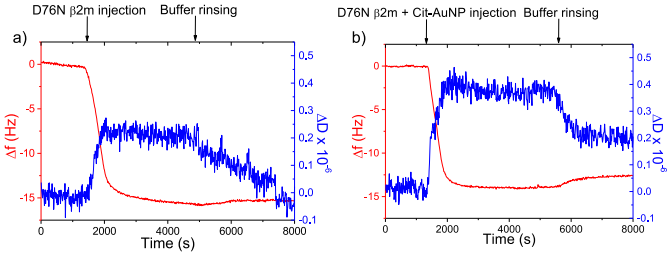

Fig. 3 Normalized frequency (red) and dissipation (blue) plots during D76N β2m adsorption onto an Au-coated QCMD sensor, a) in absence and b) in presence of Cit-AuNP. The dissipation parameter units are dimensionless.[22] For the adsorption of Cit-AuNP alone, see Figs. S10 and S11 ESI†.

Table 1 QCMD adsorption parameters at saturation, corresponding percentage variation after rinsing and associated protein surface density. The densities were calculated from Δf_{sat} values obtained by Sauerbrey fitting[21] of the data without and with Cit-AuNP.

Sample	Δf_{sat} (Hz)	ΔD_{sat} (× 10^{-6})	$\Delta f_{rinsing}$ (%)	monomers/cm²
D76N β2m	−15.7	0.16	2.5 %	14.5 ×10^{12}
D76N β2m + Cit-AuNP	−13.9	0.39	9.3 %	12.7 × 10^{12}

respect to the protein in presence of Cit-AuNP (12.7×10^{12}). In the latter case, no correction was done on the calculated surface density for Cit-AuNP adsorption (Fig. S10 ESI†). Based on the crystallographic dimensions of β2m,[23] surface coverages of 11.4×10^{12} monomers/cm² or 26.3×10^{12} monomers/cm² can be estimated for lying or standing β2m cylindroids, respectively (Fig. S12, ESI†). It can be thus inferred that D76N β2m forms essentially a single layer on the sensor surface and preferentially arranges on this surface with a parallel orientation of the β-sheets of the immunoglobulin motif. The packing density appears to be reduced in presence of Cit-AuNP. To evaluate the adsorption kinetics, a fitting of the Δ*f* time-evolution was performed according to a sigmoid Boltzmann model (Fig. 4b):

$$\Delta f = \frac{A_1 - A_2}{1 + e^{(t - t_0)/dt}} + A_2 \qquad (2)$$

where A_1 and A_2 are initial and final asymptotes, respectively, t_0 is the sigmoid centre and *dt* is the time constant of the adsorption process. The values of the adsorption time constants (*dt*) (Table 2) reveal a higher adsorption rate for the protein in presence rather than in absence of Cit-AuNP. This faster adsorption of the protein when incubated with NP can be explained in terms of a lower degree of oligomeric association that can account also for the reduced packing density reported in Table 1 and is consistent with the faster diffusion measured by NMR in presence of Cit-AuNP (Fig. 2). Another important information can be drawn from the Δ*f* data of Fig. 3. After the buffer rinsing step, a small frequency increase was measured for the protein solutions in absence

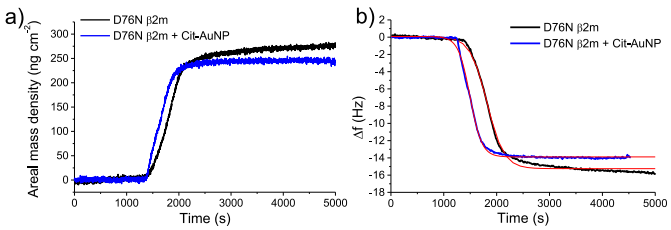

Fig. 4 a) Time course of the adsorbed mass density as obtained by the Sauerbrey equation[21] from QCMD measurements on D76N β2m without (black) and with Cit-AuNP (blue). b) Time course of the QCMD frequency changes for D76N β2m without (black) and with Cit-AuNP (blue). The red lines indicate the fitting according to Eq. (2). For Cit-AuNP alone, see Figs. S10 and S11 ESI†.

and in presence of Cit-AuNP. The quartz crystal frequency increase reflects fractional desorption or washing away of the protein from the sensor surface. According to the values of $\Delta f_{rinsing}$ (Table 1), we conclude that a small fraction of the protein molecules adsorbed on the gold surface was physisorbed and could be easily removed by rinsing, whereas most of the protein was bound more tightly by chemisorption. However, the percentage of frequency variation induced by rinsing was higher in presence of Cit-AuNP (Table 1) indicating that more protein molecules are loosely bound to the sensor surface in presence of NP.

The quartz crystal frequency shift can be associated with estimates of energy dissipation change (Fig. 3).[22] The energy dissipation is related to the viscoelastic properties of the adsorbed layer.[22] D76N β2m showed a very low dissipation increase typical of rigid systems.[22] Larger dissipation change was observed in presence of Cit-AuNP, indicating the presence of a more flexible protein layer, in agreement with the larger $\Delta f_{rinsing}$ (Table 1). This conclusion is also supported by the different overtone analysis (Fig. S11 ESI†). To relate the dissipation changes to frequency, i.e. mass deposition changes, independently of time, Δ*D* is plotted versus −Δ*f* (*D*-*f* plot)[24,25] (Fig. 5). The density of the points in *D*-*f* plots depends on the adsorption kinetics; the faster the kinetics the farther the points. The lower density of the points in the *D*-*f* plot that corresponds to the protein incubated with Cit-AuNP (Fig. 5b) confirms the faster adsorption kinetics already found with the sigmoidal fitting of Δ*f*. Moreover, the presence of a single slope in each plot confirms that there is only one kinetic process during adsorption.[24,25] The possibility of recognizing two slopes, especially for the protein with Cit-AuNP (Fig. 5b), albeit beyond the experimental error confidence, appears consistent with the adsorption mechanism proposed by Glomm *et al.*[25] The presence of a second distinct slower adsorption regime is explained with an initial adsorption where protein-surface interactions prevail,[25] followed by a phase where also protein- protein interactions become important and slow down the adsorption process, as the surfa-

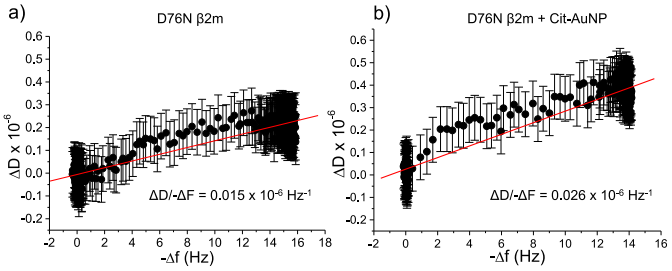

Fig. 5 *D*-*f* plots for D76N β2m a) alone and b) in presence of Cit-AuNP. The error bar corresponds to the ordinate uncertainty (1×10^{-7}).[22] The red lines represent the linear fittings and the corresponding slopes (Δ*D*/−Δ*f*) are reported on the plots.

Table 2 Parameters obtained from QCMD frequency data fitted with Boltzmann sigmoid model (Eq (2)).

Sample	A_1 (Hz)	A_2 (Hz)	t_0 (s)	dt (s)	χ^2	R^2
D76N β2m	1.14±0.16	-15.27±0.02	1788±5	180±4	0.098	0.99
D76N β2m + Cit-AuNP	3.83±0.29	-13.93±0.01	1568±6	163±2	0.017	0.99

ce coverage increases. In addition to kinetic information, the slope of *D-f* plots is related to the viscoelastic properties of the adsorbed layer.[25] As seen in Fig. 5, a higher slope can be extracted for the sample of the protein with Cit-AuNP (Fig. 5b). The larger dissipation and dissipation derivative with respect to mass deposition of the protein in presence of Cit-AuNP can be ascribed to an increase of the intermolecular (interstitial) hydration.[24] The intermolecular hydration decreases the compactness of the protein layer and therefore increases the dissipative ability of the same layer, coherently with all the other parameters of Table 1. The increase of interstitial water in presence of Cit-AuNP can be again attributed to a lower degree of protein association which, in turn, is fully consistent with the NMR evidence. It is worth of note that our experimental evidence appears to rule out the occurrence of a hard corona,[26] i.e. a stable β2m layer around Cit-AuNP. However, the presence of a few tightly-adsorbed molecules can not be excluded.

NMR and QCMD experiments show that Cit-AuNP are able to interfere with β2m protein-protein interactions (PPIs) leading to a reduction of the association equilibria. This effect was assessed not only for the wild-type variant, but also for D76N variant that displays more pronounced association in solution, in line with the enhanced amyloidogenicity.[11,12] These results suggest that Cit-AuNP can inhibit β2m PPIs. The decrease in the protein association extent is likely to be the mechanism by which Cit-AuNP hinder D76N β2m fibrillogenesis without enforcing a tight protein-NP binding.

Conflicts of interest

There are no conflicts to declare.

Notes and references

§ We thank NYUAD Core Technology Platform for the access to NMR and QCMD facilities.

1 J. Hardy and D. J. Selkoe, *Science*, 2002, **297**, 353–356.
2 H. A. Lashuel, D. Hartley, B. M. Petre, T. Walz and P. T. L. Jr, *Nature*, 2002, **418**, 291.
3 F. Chiti and C. M. Dobson, *Annu. Rev. Biochem.*, 2006, **75**, 333–366.
4 I. A. Mastrangelo, M. Ahmed, T. Sato, W. Liu, C. Wang, P. Hough and S. O. Smith, *J. Mol. Biol.*, 2006, **358**, 106–119.
5 V. H. Finder and R. Glockshuber, *Neurodegener. Dis.*, 2007, **4**, 13–27.
6 T. Eichner and S. E. Radford, *J. Mol. Biol.*, 2009, **386**, 1312–1326.
7 C. Haass and D. J. Selkoe, *Nat. Rev. Mol. Cell Biol.*, 2007, **8**, 101.
8 S. Li, S. Hong, N. E. Shepardson, D. M. Walsh, G. M. Shankar and D. Selkoe, *Neuron*, 2009, **62**, 788–801.
9 F. Gejyo, T. Yamada, S. Odani, Y. Nakagawa, M. Arakawa, T. Kunitomo, H. Kataoka, M. Suzuki, Y. Hirasawa, T. Shirahama, A. S. Cohen and K. Schmid, *Biochem. Biophys. Res. Commun.*, 1985, **129**, 701–706.
10 G. Esposito, A. Corazza, P. Viglino, G. Verdone, F. Pettirossi, F. Fogolari, A. Makek, S. Giorgetti, P. Mangione, M. Stoppini and V. Bellotti, *Biochim. Biophys. Acta*, 2005, **1753**, 76–84.
11 S. Valleix, J. D. Gillmore, F. Bridoux, P. P. Mangione, A. Dogan, B. Nedelec, M. Boimard, G. Touchard, J.-M. Goujon, C. Lacombe, P. Lozeron, D. Adams, C. Lacroix, T. Maisonobe, V. Planté-Bordeneuve, J. A. Vrana, J. D. Theis, S. Giorgetti, R. Porcari, S. Ricagno, M. Bolognesi, M. Stoppini, M. Delpech, M. B. Pepys, P. N. Hawkins and V. Bellotti, *N. Engl. J. Med.*, 2012, **366**, 2276–2283.
12 P. P. Mangione, G. Esposito, A. Relini, S. Raimondi, R. Porcari, S. Giorgetti, A. Corazza, F. Fogolari, A. Penco, Y. Goto, Y. H. Lee, H. Yagi, C. Cecconi, M. M. Naqvi, J. D. Gillmore, P. N. Hawkins, F. Chiti, R. Rolandi, G. W. Taylor, M. B. Pepys, M. Stoppini and V. Bellotti, *J. Biol. Chem.*, 2013, **288**, 30917-30930.
13 C. Cantarutti, S. Raimondi, G. Brancolini, A. Corazza, S. Giorgetti, M. Ballico, S. Zanini, G. Palmisano, P. Bertoncin, L. Marchese, P. P. Mangione, V. Bellotti, S. Corni, F. Fogolari and G. Esposito, *Nanoscale*, 2017, **9**, 3941–3951.
14 M. Mahmoudi, H. R. Kalhor, S. Laurent and I. Lynch, *Nanoscale*, 2013, **5**, 2570-2588.
15 G. Bodenhausen and D. J. Ruben, *Chem. Phys. Lett.*, 1980, **69**, 185–189.
16 F. A. A. Mulder, D. Schipper, R. Bott and R. Boelens, *J. Mol. Biol.*, 1999, **292**, 111–123.
17 G. Brancolini, A. Corazza, M. Vuano, F. Fogolari, M. C. Mimmi, V. Bellotti, M. Stoppini, S. Corni and G. Esposito, ACS Nano, 2015, **9**, 2600–2613.
18 K. F. Morris and C. S. Johnson, *J. Am. Chem. Soc.*, 1992, **114**, 3139–3141.
19 G. Esposito, M. Garvey, V. Alverdi, F. Pettirossi, A. Corazza, F. Fogolari, M. Polano, P. P. Mangione, S. Giorgetti, M. Stoppini, A. Rekas, V. Bellotti, A. J. R. Heck and J. A. Carver, *J. Biol. Chem.*, 2013, **288**, 17844–17858.
20 S. Giorgetti, S. Raimondi, K. Pagano, A. Relini, M. Bucciantini, A. Corazza, F. Fogolari, L. Codutti, M. Salmona, P. Mangione, L. Colombo, A. De Luigi, R. Porcari, A. Gliozzi, M. Stefani, G. Esposito, V. Bellotti and M. Stoppini, *J. Biol. Chem.*, 2011, **286**, 2121–2131.
21 G. Sauerbrey, *Z. Für Phys.*, 1959, **155**, 206–222.
22 M. C. Dixon, *J. Biomol. Tech. JBT*, 2008, **19**, 151–158.
23 J. W. Becker and G. N. Reeke, *Proc. Natl. Acad. Sci. U. S. A.*, 1985, **82**, 4225–4229.
24 F. Höök, M. Rodahl, P. Brzezinski and B. Kasemo, *Langmuir*, 1998, **14**, 729–734.
25 W. R. Glomm, Halskau Øyvind, A.-M. D. Hanneseth and S. Volden, *J. Phys. Chem. B*, 2007, **111**, 14329–14345.
26 M. Rahman, S. Laurent, N. Tawil, L. Yahia and Mahmoudi M. *Protein-Nanoparticle Interactions,* Springer-Verlag, Berlin Heidelberg 2013, Ch. 2.